

Assessing protein–ligand binding modes with computational tools: the case of PDE4B

Gülşah Çifci¹ · Viktorya Aviyente¹ · E. Demet Akten² · Gerald Monard^{3,4} 

Received: 9 January 2017 / Accepted: 13 May 2017 / Published online: 22 May 2017
© Springer International Publishing Switzerland 2017

Abstract In a first step in the discovery of novel potent inhibitor structures for the PDE4B family with limited side effects, we present a protocol to rank newly designed molecules through the estimation of their IC_{50} values. Our protocol is based on reproducing the linear relationship between the logarithm of experimental IC_{50} values [$\log(IC_{50})$] and their calculated binding free energies ($\Delta G_{\text{binding}}$). From 13 known PDE4B inhibitors, we show here that (1) binding free energies obtained after a docking process by AutoDock are not accurate enough to reproduce this linear relationship; (2) MM-GB/SA post-processing of molecular dynamics (MD) trajectories of the top ranked AutoDock pose improves the linear relationship; (3) by taking into account all representative structures obtained by AutoDock and by averaging MM-GB/SA computations on a series of 40 independent MD trajectories, a linear relationship between $\log(IC_{50})$ and the lowest $\Delta G_{\text{binding}}$ is achieved with $R^2 = 0.944$.

Keywords PDE4B · IC_{50} · Molecular docking · Molecular dynamics · MM-GB/SA

Introduction

The cyclic nucleotide phosphodiesterase (PDE) is an enzyme responsible for the degradation of the second messengers cyclic adenosine 3',5'-monophosphate (cAMP) and guanosine 3',5'-monophosphate (cGMP) into 5'-adenosine monophosphate (5'-AMP) and 5'-guanosine monophosphate (5'-GMP) respectively in many cell types [1–3].

The second messengers, cAMP and cGMP, are essential for many metabolic processes such as vision, muscle contraction, neurotransmission, exocytosis, cell growth, differentiation, learning, apoptosis, lipogenesis, glycogenolysis, ion channel functions and gluconeogenesis [4–7]. The regulation of the level of second messengers in vivo by synthesis activity of the receptor-linked enzymes (adenyl and guanylyl cycases) and hydrolysis into 5'-nucleotide monophosphates by PDEs is therefore of crucial importance [8–11].

Up to now, 11 families of PDE enzyme with different substrate specificity, inhibition, substrate requirements, gene sequence and tissue distribution have been reported [1, 5, 6, 12, 13]. Among these families, the cAMP specific one is PDE4, which is encoded by four different isoforms as A, B, C and D. These isoforms are characterized by unique N-terminal regions [10]. The PDE4 subfamily has attracted much attention for its usage in the treatment of inflammatory and immune disorders such as asthma, chronic obstructive pulmonary disease (COPD), rhinitis and also as therapeutic agent for rheumatoid arthritis, multiple sclerosis, type II diabetes, septic shock, atopic dermatitis, and other autoimmune diseases [14–17].

Electronic supplementary material The online version of this article (doi:10.1007/s10822-017-0024-7) contains supplementary material, which is available to authorized users.

✉ Gerald Monard
Gerald.Monard@univ-lorraine.fr

- ¹ Department of Chemistry, Boğaziçi University, 34342 Bebek, Istanbul, Turkey
- ² Bioinformatics and Genetic, Kadir Has University, 34083 Cibali, Istanbul, Turkey
- ³ Université de Lorraine, UMR 7565 SRSMC, Boulevard des Aiguillettes, B.P. 70239, 54506 Vandoeuvre-les-Nancy, France
- ⁴ CNRS, UMR 7565 SRSMC, Boulevard des Aiguillettes, B.P. 70239, 54506 Vandoeuvre-les-Nancy, France

In the PDE4 subfamily, among the four isoforms A, B, C and D, PDE4B has a specific importance especially in the inflammatory responses of lymphocytes [9]. The design of novel inhibitors for PDE4B is of significant interest to the pharmaceutical industry due to its usage as an attractive target for anti-inflammatory diseases. There are many PDE4 inhibitors that have been under clinical trials [9, 10, 18] however their clinical utility has often been limited due to their side effects like vomiting, nausea and increased gastric secretion [19]. It is thus important to design a novel PDE4B selective inhibitor with reduced side effects and improved pharmacological profile.

Designing small molecules with desirable binding affinity and biological activity is one of the major goals in computational biology [20–23]. Molecular docking is a popular method used to identify the orientations of molecules into the active site of a target protein structure [24, 25]. In the last years, docking methods have been improved by adding energy contributions or by refining the parameters for scoring functions but there are still some limitations especially like sometimes poor correlation between docking score values and experimental binding affinities [21, 23]. Up to now, many studies involving molecular docking, molecular modeling, pharmacophore modeling, the investigation of the hydrolysis mechanism and the description of the structure-activity relationships for PDE4 inhibitors have been published. Different series of PDE4 selective inhibitors have been studied by Alexander et al. [26], Kuang et al. [27], Ke et al. [28], Guay et al. [29], Xu et al. [30], Wierzbicki et al. [31] and Zhan et al. [32] have focused on the hydrolysis mechanism of PDE4 enzyme. In 2002, Colicelli et al. [33] have carried out a molecular docking study of competitive PDE inhibitors. Another molecular docking study with development of an empirical binding free energy for PDE4 inhibitors in 2006 was performed by Barreiro et al. [34], Zhu et al. [35] have combined multiple pharmacophore modeling and molecular docking process to suggest novel PDE4 inhibitors. Another pharmacophore modeling study for PDE4 was carried out by Gu et al. [36] However, to the best of our knowledge, no study based on performing molecular dynamics (MD) simulations and calculating free binding energies with different methods for PDE4 family has been reported so far with the notable exception of the work of Zhao et al. [37] on PDE4D where they have combined molecular docking, MD simulations, binding free energy, and bioassay on three natural resveratrol analogs.

In this context, an important goal of computational medicinal chemistry is to develop methods that can accurately estimate the free energy of binding, $\Delta G_{\text{binding}}$, and that could allow the estimation of the binding strength of any drug candidate prior to its synthesis. The free binding energies can be represented as:

$$\Delta G_{\text{binding}} = RT \log K_i \quad (1)$$

where R is the ideal gas constant, T is the temperature, and K_i is the dissociation constant of the enzyme–inhibitor complex. The K_i constant can be related to experimental IC_{50} values based on the following equation [38, 39]:

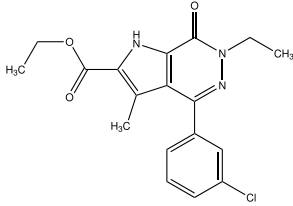
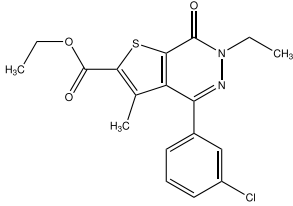
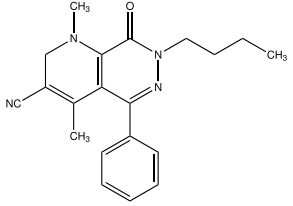
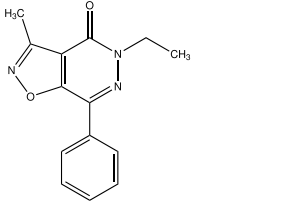
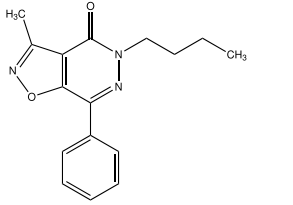
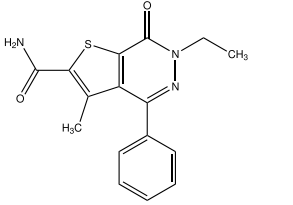
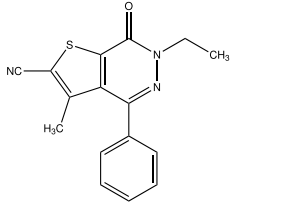
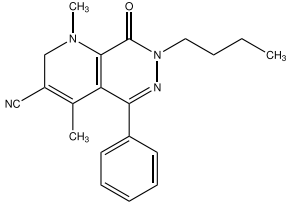
$$K_i = \frac{IC_{50}}{1 + \frac{[S]}{K_m}} \quad (2)$$

From Eq. 2 the binding affinity K_i depends on the IC_{50} value, the substrate concentration $[S]$ and the Michaelis–Menten constant K_m . For a set of ligands and their experimentally measured IC_{50} , there should therefore be a linear dependency between K_i and IC_{50} provided that the experimental conditions for all ligands are similar: the substrate concentration should be identical for all experiments and the thermodynamical conditions should remain similar (i.e., temperature, pressure, pK_a , etc.). From this point of view, a linear trend between $\Delta G_{\text{binding}}$ and $\log(IC_{50})$ values should be expected.

There are many computational approaches for free energy calculation such as free energy perturbation (FEP) [40], thermodynamic integration (TI) [41], linear response (LR) [42], Molecular mechanics-generalized born/surface area (MM-GB/SA) and Molecular Mechanics-Poisson Boltzmann/Surface Area (MM-PB/SA) methods [43, 44]. Among these methods, the most accurate and rigorous ones are FEP and TI [45]. Despite their accuracy, they have found little use in drug design [46] due to their convergence only for rather similar ligands and computational cost [47]. The MM-GB/SA and MM-PB/SA methods, that combine molecular mechanics energy and implicit solvation models, are simple and faster than FEP [23]. Therefore, they have been widely used in free energy calculations in computational medicinal chemistry [20, 21]. It is important to achieve statistically fully converged results and statistical estimates in order to test how well the methods reproduce the experimental data. As Genheden and Ryde have shown, converged results using MM-GB/SA method can be achieved by running multiple independent short MD simulations starting with different initial velocities and a same initial structure rather than by running a single (very) long simulation [47].

In this project, the aim is to evaluate binding energies with the MM-GB/SA method and show the correlation between the binding energies and half maximal inhibitory concentration (IC_{50}) values of the ligands. The study includes (i) building a database of experimental IC_{50} values that include a training and a test set; (ii) performing docking process for each ligand, (iii) carrying out independent MD simulations for the top ranked poses of each ligand and calculating the free binding energy using the

Table 1 Ligand names, 2D chemical sketches and experimental IC₅₀ values for the training set

Training set					
Ligand	2D structure	IC ₅₀ (μM)	Ligand	2D structure	IC ₅₀ (μM)
ligand3		0.6 ± 0.1 ^a	ligand4		0.9 ± 0.2 ^a
ligand5		1.1 ± 0.4 ^a	ligand6		9 ± 0.8 ^a
ligand7		6 ± 0.5 ^a	ligand8		3 ± 0.5 ^a
ligand9		4 ± 0.5 ^a	ligand10		2 ± 0.5 ^a

^aRef. [48]

MM-GB/SA approach, (iv) analyzing the role of the possible alternative poses of each ligand from MM-GB/SA calculations and finally, (v) applying a linear regression method on the training set to establish a relationship between calculated $\Delta G_{\text{binding}}$ and experimental $\log(\text{IC}_{50})$ and verifying the reliability of our approach with the test set.

Methodology

Training and test sets

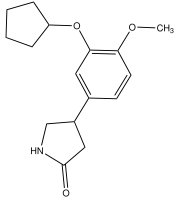
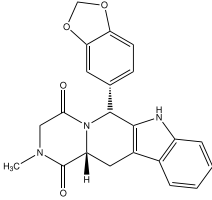
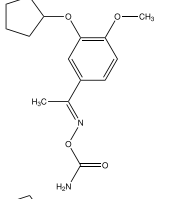
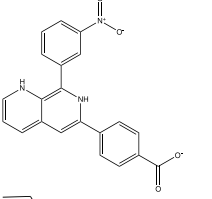
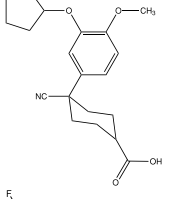
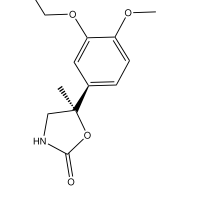
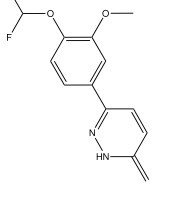
For the dataset preparation, the ligands with known IC₅₀ values from experimental studies of Dal Piaz et al. [48] and Zhang et al. [9] were chosen due to their selectivity for PDE4B and their large range of different IC₅₀ values. These

ligands were also searched in the BindingDB [49] and it was found that some of them have more than one IC₅₀ value reported, as the ligands cilomilast and npv (see Tables 1, 2). The training set has been designed to contain IC₅₀ values from a single source: those of Dal Piaz et al. It contains eight ligands for which experimental IC₅₀ values range from 0.6 to 9.0 μM. The test set contains seven molecules: rolipram, tadalafil, flaminast, mesopram, zardaverine, cilomilast and npv. Their experimental IC₅₀ values range from 0.025 to 9.2 μM.

Protein and dataset preparation

The starting structure for the protein is the human PDE4B enzyme (Protein Data Bank entry 1RO6, 2 Å resolution, see Fig. 1). The X-ray structure contains two identical chains with rolipram as a co-crystallized ligand and two

Table 2 Ligand names, 2D chemical sketches and experimental IC₅₀ values for the test set

Test set					
Ligand	2D structure	IC ₅₀ (μM)	Ligand	2D structure	IC ₅₀ (μM)
rolipram		0.32±0.09 ^a	tadalafil		9.2 ^b
filaminast		0.96 ^b	npv		0.049±0.007 ^c (0.650 ^d)
cilomilast		0.025 ^b (0.31) ^c	mesopram		0.42 ^b
zardaverine		0.93 ^b			

IC₅₀ values in parentheses are higher values reported in the BindingDB (see text)

^aRef. [48]

^bRef. [9]

^cRef. [51]

^dRef. [52]

metal ions: Zn²⁺ and Mg²⁺. All our calculations were carried out on one single active chain which includes the two metal ions, Zn²⁺ and Mg²⁺, and the water molecule (residue #788 in 1RO6) positioned between these two atoms. The choice of using the 1RO6 X-ray structure over other available PDE4B X-ray structures like the apo one (PDB entry 1FOJ) was dictated by the fact that the two structures are very similar (the RMSD between the backbones of 1RO6 and 1FOJ is only 0.13 Å) and that the docking procedure always yielded lower binding energies for 1RO6 than for 1FOJ (see Supporting Information).

The ligand dataset is a combination of training and test sets (Tables 1, 2). The IC₅₀ values of the ligands are known from different experimental studies [9, 48, 51, 52]. The training set contains molecules that have been experimentally tested using a single source: guinea pig ventricular tissue [48]. The test set contains ligands which have been tested for inhibition using PDE4B proteins from various sources: guinea pig [48], human [9, 52], or rat [51]. All these protein sources share a strong sequence homology (>95% of identity). For example, the sequence alignment between guinea pig and human PDE4B in UniProt [53] has shown that they differ by only five residues that are out of the active site.



Fig. 1 Cartoon representation of PDE4B X-ray structure generated with PyMOL [50]. Chain A is represented in *green* as cartoon, the co-crystallized ligand as ball and stick, Zn^{2+} and Mg^{2+} are in *purple*, the water molecule is depicted in *red* color

Docking procedure

The docking process was carried out with AutoDock v4.2 [54]. For each ligand, ten independent runs were performed. A pre-calculated three-dimensional energy grid of equally spaced discrete points was generated prior to the docking using the program AutoGrid [54]. The grid box ($32 \text{ \AA} \times 72 \text{ \AA} \times 31 \text{ \AA}$) contains the active site and several key residues important for the protein-ligand interaction. The distance between two grid points was set to 0.375 \AA . The grid map files were calculated by AutoGrid for the ligand atom types: A, NA, C, OA, and N. Gasteiger charges and solvation parameters were assigned using ADT [54]. For conformational search, Lamarckian Genetic Algorithm, which combines a local search and a genetic algorithm to provide both efficient global space coverage and local search optimization, was chosen. During the process, the protein was held rigid. The population size was set to 150, the maximum number of energy evaluations was set to 2,500,000, the maximum number of generations was 27,000, the mutation rate was 0.02 and the crossover rate was 0.8. The remaining parameters were set as the default values.

At the end of each docking process, the ten docked poses of each ligand were clustered based on their RMSD values using a cluster RMSD threshold of 0.5 \AA . For each cluster of each ligand, a representative pose with the lowest $\Delta G_{\text{binding}}$ value was selected and incorporated in our

analysis in order to take into account the diversity of the binding modes.

MD simulations

Ligand atomic charges were calculated with the restrained electrostatic potential fit (RESP) method at the B3LYP/cc-pVTZ level after a full geometrical optimization carried out at the B3LYP/6-31G* level. This procedure is compatible with the charges obtained for the Amber force field [55] used in the subsequent MD runs.

Hydrogen atoms were added to the system with the tleap module of AMBER 12 [56]. For histidines, the protonation state was determined based on PROPKA [57] calculations and hydrogen bond pattern analysis. Counter sodium ions were added to neutralize the system. Waters from the crystal structure were deleted except for the water molecule that is located between the two metal ions Zn^{2+} and Mg^{2+} and is hydrogen bonded to the co-crystallized ligand rolipram. The system was solvated with TIP3P [58] water molecules extending to at least 10 \AA from the protein. The system was cubic with edge length 74.50 \AA and had an initial density of 1.0 g cm^{-3} .

The MD simulations were performed using the CUDA version [59, 60] of the PMEMD module of AMBER 12. The Amber ff03 [55] force field was used to model the PDE4B protein while the general AMBER force field (GAFF) [61] force field parameters were used to model the ligands. The SHAKE [62] algorithm was chosen to constrain bond lengths involving hydrogen atoms. The Andersen temperature coupling algorithm was applied to ensure a constant temperature (NVT) ensemble. The time step was set to 2 fs.

In gas phase, before the solvation of the system, a short minimization followed by one MD run was carried out for 100 ps at 10 K to optimize the hydrogen atom positions: all heavy atoms were restrained to their crystallographic positions using a harmonic potential with a force constant of $100 \text{ kcal mol}^{-1} \text{ \AA}^{-2}$. After solvation, the equilibration of the system was performed in five stages [63]. First, only the hydrogen atoms of the system were allowed to move during 100 ps at 10 K (i.e., by applying a force constant of $50 \text{ kcal mol}^{-1} \text{ \AA}^{-2}$ on all heavy atom positions). Second, the water molecules were allowed to move for the next 100 ps at the same temperature. Third, the force constant on the protein heavy atom positions was decreased to $5 \text{ kcal mol}^{-1} \text{ \AA}^{-2}$ for another 100 ps. Then the whole system was free to move during 100 ps at 10 K. Finally, the thermostat temperature was smoothly increased from 10 to 300 K for another 2 ns.

After equilibration, for each ligand representative of its cluster, forty independent simulations were performed up to 1 ns at 300 K with different initial velocities. During the

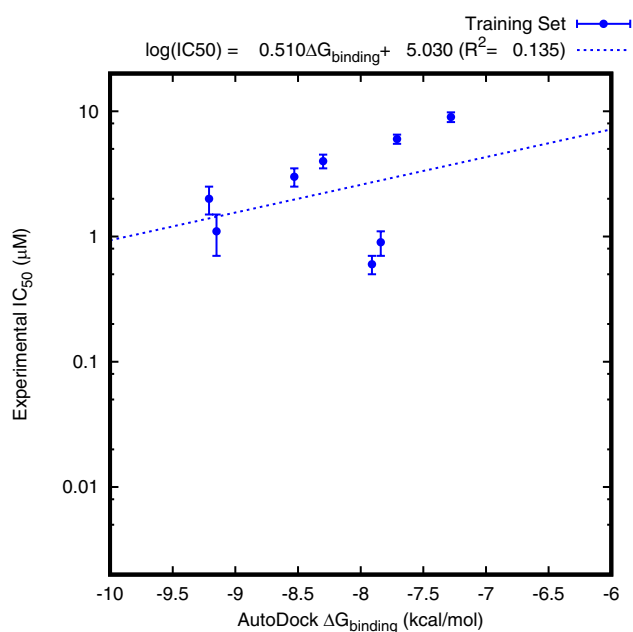


Fig. 2 Correlation between experimental IC_{50} values and the lowest ΔG scores, in kcal mol^{-1} , obtained by a series of AutoDock docking computations of the training set (in blue). Vertical error bars represent standard experimental deviations. Blue dashed line linear fit between lowest AutoDock $\Delta G_{\text{binding}}$ values and experimental $\log(IC_{50})$

production runs, coordinates were saved every 2 ps for the subsequent MM-GB/SA calculations. Using NVIDIA Tesla M2090 GPU, one 1 ns simulation takes in average 1.2 h for a speed of about 20 ns/day.

MM-GB/SA post-processing

The free energy of binding for each ligand is calculated using the equation:

$$\Delta G_{\text{binding}} = \langle G_{RL} \rangle - \langle G_R \rangle - \langle G_L \rangle \quad (3)$$

where RL, R and L stand for receptor–ligand complex, receptor and ligand, respectively. The average free energy of each system is estimated as a sum of three terms:

$$G = E_{MM} + G_{\text{solv}} - TS_{MM} \quad (4)$$

where E_{MM} is the molecular mechanics energy of each system, including internal, non-bonded electrostatics, and van der Waals energies. G_{solv} is the solvation energy which consists of a polar and a nonpolar part. The polar solvation free energy is calculated by a Generalized Born (GB) approach. The nonpolar solvation free energy is computed by a relation to the solvent-accessible surface area (SASA). The last term TS_{MM} is the product of absolute temperature and the entropy.

In this study, the first two terms were calculated using the MMPBSA.py module of AMBER 12 with all water

molecules stripped off [64]. To evaluate the polar solvation free energy, different solvation models have been evaluated: GB^{HCT} [65–67], GB^{OBC} [68], $GB^{\text{OBC-2}}$ [56, 68], GB^{GBneck} [69], and GB^{GBneck2} [70]. The hydrophobic contribution has been approximated by the Linear Combinations of Pairwise Overlaps (LCPO) method [71].

In this study, the entropy term was not included in our calculations although it could have been evaluated through a usual normal-mode analysis [72]. There have been much debate in the literature about the entropy term in MM-GB/SA calculations and whether it should be systematically included or not to improve the accuracy of the results [73–77]. In our case, given the high computational cost of its calculation and the good prediction that we have obtained without including it, we have neglected the entropy term component.

Finally, the calculated $\Delta G_{\text{binding}}$ values are averaged over 40 independent simulations for each ligand.

Results and discussion

Best docking scores versus experimental IC_{50} values

The study has started with the docking process of all ligands in both datasets into the target PDE4B enzyme using AutoDock v4.2. For each ligand, ten poses are obtained from a total of ten docking runs. The best (i.e., top ranked) pose with the lowest AutoDock $\Delta G_{\text{binding}}$ value is recorded and a linear correlation between the $\Delta G_{\text{binding}}$ and $\log(IC_{50})$ is searched for.

In Fig. 2, the correlation between the lowest AutoDock $\Delta G_{\text{binding}}$ values and the corresponding $\log(IC_{50})$ values is represented for the training set. Only a weak linear correspondence exists between $\Delta G_{\text{binding}}$ and experimental $\log(IC_{50})$ with R^2 value of 0.135. That means that, while AutoDock is capable of discriminating between different poses and of finding true positive hits, its scoring function is not capable of estimating experimental $\Delta G_{\text{binding}}$ values in the case of PDE4B.

Convergence of the free energy results

Another way to obtain binding free energies is to use the MM-GB/SA approach. Here, $\Delta G_{\text{binding}}$ energies are obtained by post-processing MD trajectories of complexed protein:ligand structures. In our cases, we have used as starting structures for the MD runs, the complexed structures obtained by AutoDock. For each docked pose, we have performed 40 independent 1 ns MD runs. The convergence of $\Delta G_{\text{binding}}$ calculations for two independent runs corresponding to the ligand rolipram is represented in Fig. 3a. It shows that a 1 ns trajectory is enough to ensure

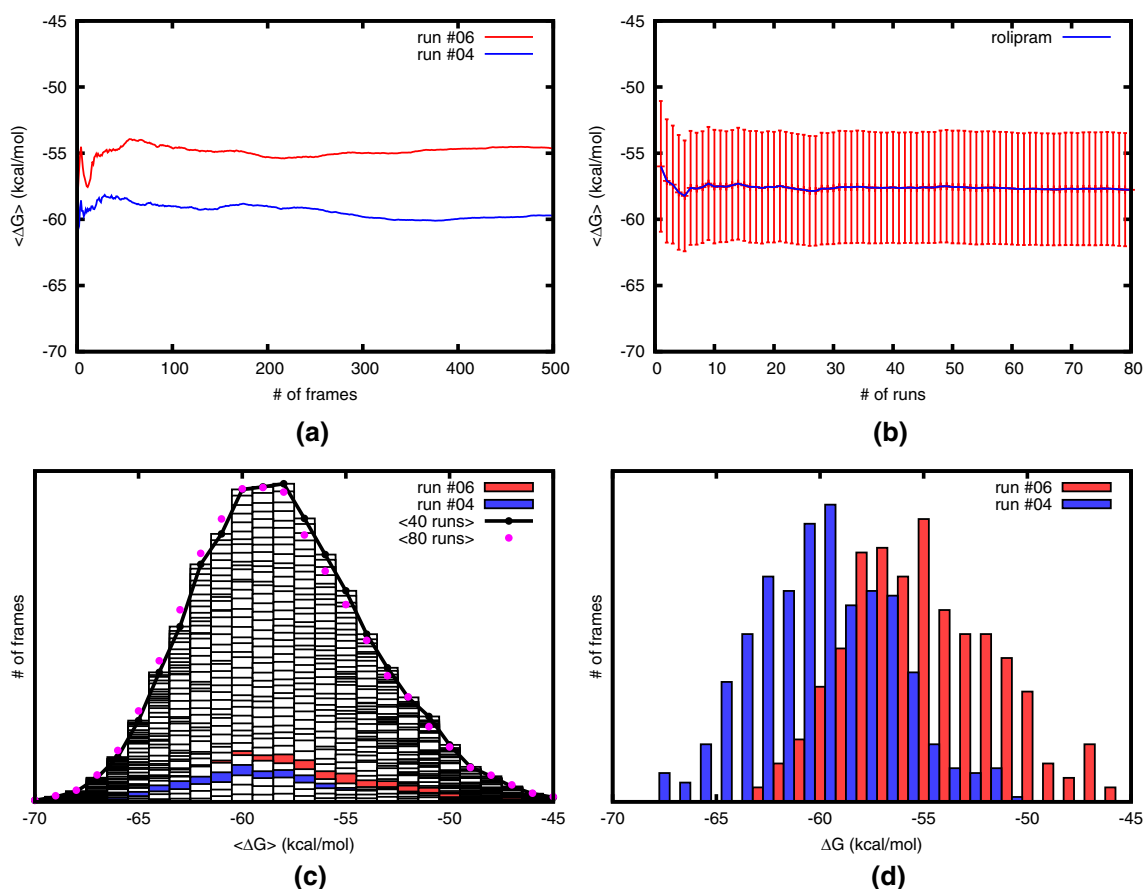


Fig. 3 Convergence of the $\Delta G_{\text{binding}}$ MM-GB/SA computations for rolipram using multiple MD trajectories. **a** Convergence of the averaged $\Delta G_{\text{binding}}$ in kcal mol⁻¹, for two independent runs of 1 ns (500 frames each); **b** convergence of the averaged $\Delta G_{\text{binding}}$ in kcal mol⁻¹, as a function of the number of independent 1 ns long MD trajectories, the error bars represent the standard deviation in kcal mol⁻¹; **c** *bulleted dark line*: Distribution of $\Delta G_{\text{binding}}$ values, in kcal mol⁻¹, after

averaging 40 independent MD runs, *magenta bullets*: distribution of $\Delta G_{\text{binding}}$ values after averaging 80 independent MD runs, *white filled rectangles*: contribution of each 40 MD run to the averaged $\Delta G_{\text{binding}}$ distribution, *blue filled rectangles*: contribution of run #04 to the averaged $\Delta G_{\text{binding}}$ distribution, *red filled rectangles*: contribution of run #06 to the averaged $\Delta G_{\text{binding}}$ distribution. **d** Distribution of $\Delta G_{\text{binding}}$ values, in kcal mol⁻¹, for two independent runs

the convergence of $\Delta G_{\text{binding}}$ for that run. However, two independent runs can give rather different results: one MD yields $\Delta G_{\text{binding}} = -54.6 \pm 3.6$ kcal mol⁻¹ while the other yields $\Delta G_{\text{binding}} = -60.5 \pm 3.4$ kcal mol⁻¹. As suggested by Genheden and Ryde [47], converged MM-GB/SA results can be obtained by averaging multiple independent trajectories. Figure 3b represents the convergence of MM-GB/SA $\Delta G_{\text{binding}}$ energies for rolipram as a function of the number of independent trajectories. Convergence is obtained after 40 trajectories (-57.6 ± 1.6 kcal mol⁻¹). Adding more trajectories do not change the picture beyond: $\Delta G_{\text{binding}} = -57.8 \pm 1.6$ kcal mol⁻¹ after 80 runs. Figure 3c represents the distribution of free energies that are obtained by cumulating all MM-GB/SA $\Delta G_{\text{binding}}$ for all runs. The contribution of the two independent runs as depicted in Figure 3d is also represented. This shows that by cumulating independent MD runs, our $\Delta G_{\text{binding}}$ values are converged. In the following steps, all MM-GB/SA free energies will be

calculated for every distinct ligand pose representative of each cluster using the same protocol: the MM-GB/SA post-processing of 40 independent MD runs using different random initial velocities associated to the structure coordinates of the corresponding pose as obtained by AutoDock.

MM-GB/SA binding free energies of top ranked AutoDock poses versus experimental IC₅₀ values

The $\Delta G_{\text{binding}}$ values have been calculated using the MM-GB/SA approach for the top ranked poses of all ligands in the training set and the test sets. Figure 4 represents the correlation between $\Delta G_{\text{binding}}$ and the logarithm of the experimental IC₅₀. For the training set, the linearity of the trend is more pronounced ($R^2 = 0.788$) than when using the AutoDock scores ($R^2 = 0.135$). This shows that using a molecular force field as the AMBER force field yields more accurate results.

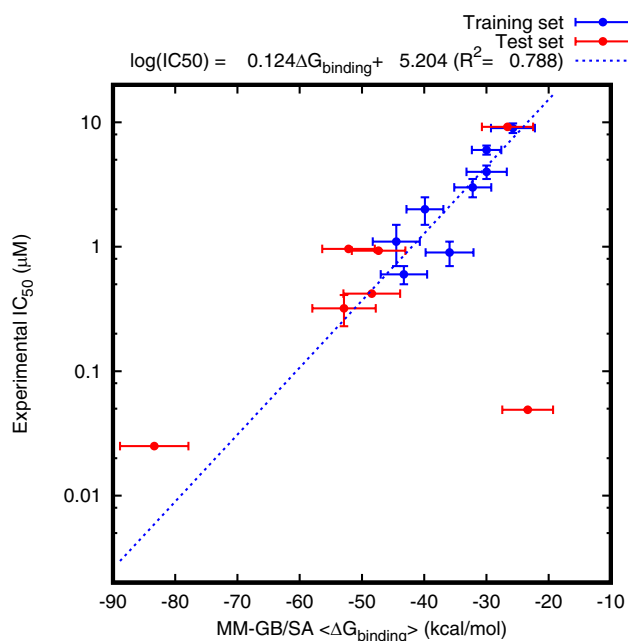


Fig. 4 Correlation between experimental IC_{50} values and MM-GB/SA averaged $\Delta G_{\text{binding}}$ free energies computed from the top ranked AutoDock poses of the training set (in blue) and the test set (in red). Vertical error bars represent standard experimental deviations. Horizontal error bars represent computed standard $\Delta G_{\text{binding}}$ deviations. Blue dashed line: linear fit between $\Delta G_{\text{binding}}$ values for the top ranked AutoDock poses and experimental $\log(IC_{50})$

When the test set is assessed (Fig. 4, error bars in blue), most $\Delta G_{\text{binding}}$ values are correlated to their experimental IC_{50} counterparts as in the training set. However, one value is off the linear region by more than 50 kcal mol⁻¹. This corresponds to the npv ligand for which two IC_{50} values have been reported: 0.049 (Ref. [51]) and 0.650 (Ref. [52]). Given the linear trend of the binding free energies found for the training set, from these two IC_{50} values should correspond two possible $\Delta G_{\text{binding}}$: one around -66.3 kcal mol⁻¹, the other around -45.4 kcal mol⁻¹. Using the top ranked AutoDock pose, the MM-GB/SA binding free energy is computed at -23.4 ± 4.1 kcal mol⁻¹ instead.

Minimum MM-GB/SA binding free energies versus experimental IC_{50} values

If MM-GB/SA $\Delta G_{\text{binding}}$ values are better correlated to experimental IC_{50} values than AutoDock $\Delta G_{\text{binding}}$ values, one can wonder whether alternative poses obtained by AutoDock would be ranked similarly if the docking score was obtained from a MM-GB/SA computation instead. While we cannot change the way AutoDock optimizes the poses during molecular docking, we have performed MM-GB/SA calculations on a more diverse set of poses: one representative pose of each cluster for each ligand in

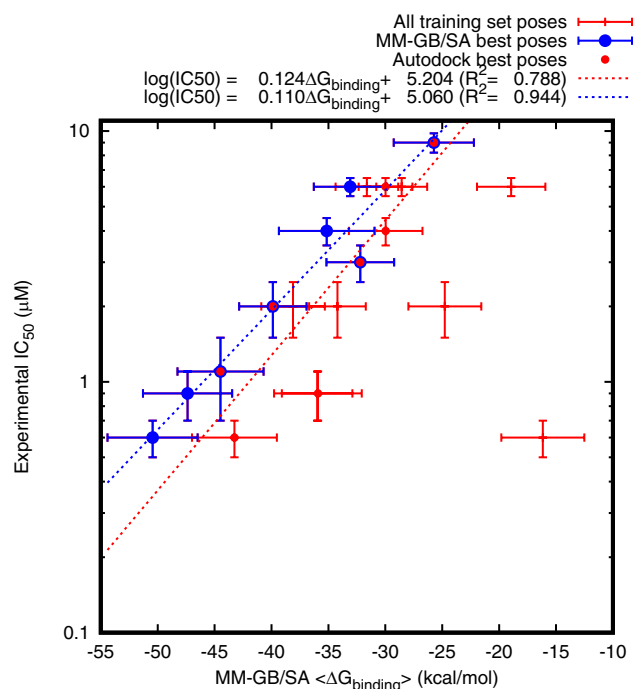


Fig. 5 Correlation between experimental IC_{50} values of the training set and MM-GB/SA averaged $\Delta G_{\text{binding}}$ free energies computed for all AutoDock poses (one representative pose per AutoDock family). Vertical error bars represent standard experimental deviations. Horizontal error bars represent computed standard $\Delta G_{\text{binding}}$ deviations. Red filled circles $\Delta G_{\text{binding}}$ values corresponding to the top ranked AutoDock poses. Blue filled circles minimum $\Delta G_{\text{binding}}$ values. Red dashed line linear fit between $\Delta G_{\text{binding}}$ values for the top ranked AutoDock poses and experimental $\log(IC_{50})$. Blue dashed line linear fit between minimum $\Delta G_{\text{binding}}$ values and experimental $\log(IC_{50})$

the training set was chosen and MM-GB/SA $\Delta G_{\text{binding}}$ was computed using the same multiple MD trajectory approach than for the top ranked AutoDock pose. The number of alternative poses per ligand in the training set varies from 1 (e.g., ligand5) to 5 (e.g., ligand7).

In Fig. 5, the correlation between the calculated $\Delta G_{\text{binding}}$ and the experimental IC_{50} values is represented. For some ligands, a lower $\Delta G_{\text{binding}}$ value than for the top ranked AutoDock pose is found. When the minimum averaged $\Delta G_{\text{binding}}$ values are used (blue filled circles in Fig. 5), a better linear trend is found than when only top ranked AutoDock poses are considered (red filled circles in Fig. 5). The relationship between computed averaged $\Delta G_{\text{binding}}$ and experimental $\log(IC_{50})$ is expressed as:

$$\log(IC_{50}) = 0.110\Delta G_{\text{binding}} + 5.060 \quad (5)$$

with a correlation coefficient $R^2 = 0.944$

The improvement of the correlation coefficient shows that while AutoDock is capable of discriminating

Table 3 Linear fitting results, estimated IC₅₀, in μM, for all approaches and comparison with experimental values

Method	AutoDock	MM-GB/SA						
	Top ranked	Top ranked	min Δ <i>G</i>					
GB model		OBC ^b	HCT ^a	OBC ^b	OBC-2 ^c	GBneck ^d	GBneck2 ^e	
a	0.510	0.124	0.106	0.110	0.104	0.085	0.042	
b	5.030	5.204	5.214	5.060	4.982	4.361	2.975	
R ²	0.135	0.788	0.929	0.944	0.945	0.892	0.780	
Molecule	Estimated IC ₅₀ for the training set							Exp. IC ₅₀
Ligand3	2.7	0.8 ± 0.3	0.6 ± 0.2	0.6 ± 0.2	0.7 ± 0.2	0.7 ± 0.2	0.8 ± 0.2	0.6 ± 0.1 ^f
Ligand4	2.8	2.1 ± 0.8	0.9 ± 0.3	0.9 ± 0.3	1.0 ± 0.3	1.1 ± 0.4	1.1 ± 0.2	0.9 ± 0.2 ^f
Ligand5	1.4	0.7 ± 0.3	1.3 ± 0.4	1.2 ± 0.4	1.1 ± 0.4	0.9 ± 0.3	0.9 ± 0.2	1.1 ± 0.4 ^f
Ligand6	3.7	7.4 ± 2.6	8.7 ± 2.7	9.4 ± 3.0	10.0 ± 3.1	9.4 ± 2.3	6.7 ± 0.9	9.0 ± 0.8 ^f
Ligand7	3.0	4.4 ± 1.1	4.1 ± 1.1	4.2 ± 1.2	4.2 ± 1.2	4.4 ± 1.1	4.9 ± 0.6	6.0 ± 0.5 ^f
Ligand8	2.0	3.3 ± 1.0	4.7 ± 1.2	4.6 ± 1.3	4.4 ± 1.2	4.8 ± 1.1	4.7 ± 0.6	3.0 ± 0.5 ^f
Ligand9	2.2	4.4 ± 1.5	3.2 ± 1.1	3.3 ± 1.2	3.3 ± 1.2	2.4 ± 0.8	1.9 ± 0.5	4.0 ± 0.5 ^f
Ligand10	1.4	1.3 ± 0.4	2.3 ± 0.6	2.0 ± 0.6	1.9 ± 0.5	2.2 ± 0.6	3.4 ± 0.5	2.0 ± 0.5 ^f
MAPE (%)	101.7	38.5	19.5	15.1	16.5	24.4	38.4	
Molecule	Estimated IC ₅₀ for the test set							Exp. IC ₅₀
Tadalafil	2.3	6.7 ± 2.7	7.7 ± 2.8	8.5 ± 3.1	7.2 ± 2.7	5.6 ± 1.7	4.1 ± 0.8	9.2 ^g
Rolipram	2.38	0.25 ± 0.12	0.36 ± 0.12	0.48 ± 0.20	0.42 ± 0.18	0.98 ± 0.37	0.29 ± 0.06	0.32 ± 0.09 ^f
Filaminast	3.15	0.28 ± 0.11	0.35 ± 0.12	0.52 ± 0.19	0.45 ± 0.16	0.33 ± 0.12	0.36 ± 0.07	0.96 ^g
Mesopram	4.59	0.44 ± 0.19	0.62 ± 0.21	0.78 ± 0.31	0.70 ± 0.27	0.89 ± 0.37	0.51 ± 0.12	0.42 ^g
Zardaverine	5.41	0.51 ± 0.21	0.87 ± 0.31	0.88 ± 0.33	0.86 ± 0.31	1.11 ± 0.36	0.59 ± 0.11	0.93 ^g
Cilomilast	0.239	0.006	0.006	0.017	0.013	0.035	1.2 × 10 ⁻⁰⁴	0.025 ^g
		±0.003	±0.003	±0.008	±0.006	±0.014	±4.9 × 10 ⁻⁰⁵	(0.31 ^h)
Npv	0.342	9.962	0.023	0.022	0.011	0.012	0.002	0.049 ± 0.007 ^h
		±3.964	±0.010	±0.011	±0.006	±0.006	±0.001	(0.650 ⁱ)
MAPE (%)	553.6	2925.5	38.8	40.1	43.6	79.5	54.4	

^aRef. [65–67]^bRef. [68]^cRef. [56, 68]^dRef. [69]^eRef. [70]^fRef. [48]^gRef. [9]^hRef. [51]ⁱRef. [52]

between bad and good binding poses, its docking scores are not quantitative enough to be used directly to evaluate the binding affinity of a ligand for PDE4B. However, by using the many different poses extracted from AutoDock runs and by applying a protocol that involves MM-GB/SA calculations on multiple independent trajectories, it is possible to recover correct Δ*G*_{binding} values that are in quantitative agreement with experimental values.

Estimation of IC₅₀ values

Using Eq. 5, it is now possible to estimate IC₅₀ values from MM-GB/SA Δ*G*_{binding} values. Table 3 summarizes all the results that have been obtained for the test set and the training set when applying one of the three computational approaches presented here: (i) linear fitting using the AutoDock Δ*G* scores of the top ranked poses; (ii) linear fitting using averaged MM-GB/SA values for the top ranked AutoDock poses; (iii) linear fitting using the

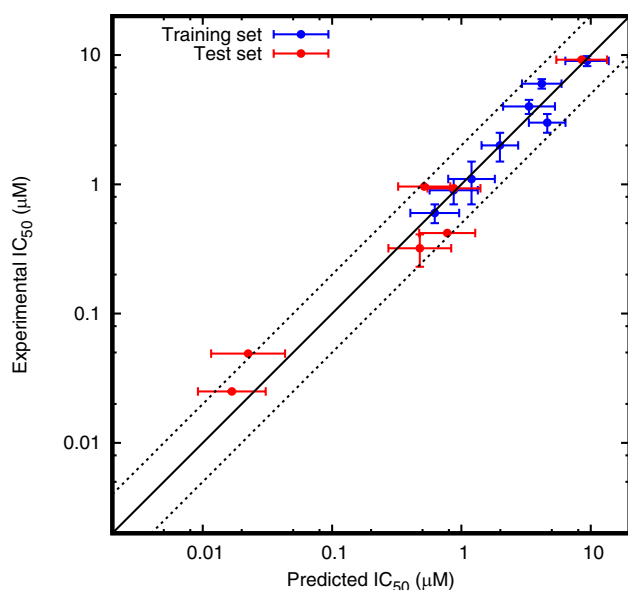


Fig. 6 Correlation between experimental IC_{50} values and estimated IC_{50} values obtained after fitting averaged MM-GB/SA free energies computed from all AutoDock poses (1 represent per family) using the GB^{OBC} model. *blue*: training set, *red*: test set. *Vertical error bars* represent standard experimental deviations. *Horizontal error bars* represent standard estimated deviations. *Black line* represents an ideal estimation while *dashed lines* represent an error factor of 2 (*upper dashed line*) or 0.5 (*lower dashed line*) in the estimated IC_{50} value, respectively

lowest averaged MM-GB/SA values among representative poses of all AutoDock clusters. Because IC_{50} values are spread in an exponential range from 0.025 to 9.2 μM , we use mean absolute percentage error (MAPE) as a criterion to evaluate the error between experimental IC_{50} values and estimated IC_{50} values. MAPE numbers, expressed as percentage, are calculated using the following expression:

$$\text{MAPE} = \frac{1}{N} \sum_{i=1}^N \left| \frac{IC_{50}^{\text{est}} - IC_{50}^{\text{exp}}}{IC_{50}^{\text{exp}}} \right| \quad (6)$$

where IC_{50}^{est} and IC_{50}^{exp} are the estimated and the experimental IC_{50} values for molecule i , respectively.

Figure 6 shows the correlation between estimated IC_{50} values using the GB^{OBC} model and experimental IC_{50} values for both the training set used to define Eq. 5 and the test set. By using all AutoDock clusters, the estimated IC_{50} values from the test set are within 38% of relative error (see Table 3). Like in the training set, the use of distinct AutoDock poses improves the estimation significantly and no ligand from the test set are wrongly estimated as it was the case when only the top ranked AutoDock poses were considered (Fig. 4).

From Table 3 and Figure S1b, IC_{50} prediction using the AutoDock scores gives a MAPE of 101.7% for the training set and 553.6% for the test set, respectively. As stated above, AutoDock ΔG values show a linear trend but the correlation is not strong ($R^2 = 0.135$, Figure S1). When using the GB^{OBC} model on the top ranked AutoDock poses, the agreement between experimental and predicted IC_{50} values is improved ($R^2 = 0.788$, MAPE= 38.5% for the training set). However, some ligands like npv are wrongly predicted. This yields a MAPE of 2925.5% for the test set. By adding alternative poses, the agreement for the training set is much better, yielding $R^2 = 0.944$ and MAPE= 15.1%. Test ligands, including npv (see below), are now correctly predicted with a MAPE of around 40%. The GB^{OBC} model is the one that leads to the best prediction. But other GB/SA models like GB^{HCT} , $GB^{\text{OBC-2}}$, and GB^{GBneck} also give reliable predictions and are always superior than the approach which uses only the top ranked AutoDock poses (see Supplementary Information). Surprisingly, the GB^{GBneck2} model yields the worst results among all GB/SA models. This was not expected since it is one of the most recent GB/SA model and it has proved to be accurate in modeling solvent effects in protein folding studies [78]. At the same time, GB^{GBneck2} is the GB/SA model that yields to the smallest standard error when using multiple MD trajectories (Figure S6).

Finally, one important question that arises from those results is to check if our current protocol is capable of discriminating between experimental values when several are available in the literature. This is the case for cilomilast and npv. Surprisingly, these two molecules are the only two of our sets that contain a carboxylate group. The results reported Table 3 have been obtained when the carboxylate form was considered. We have recomputed predicted IC_{50} values for the carboxylic acid form for both molecules (see Supporting Information for full results). For cilomilast and using the GB^{OBC} model, the predicted IC_{50} values for the carboxylate and the carboxylic acid forms are 0.017 ± 0.008 and 0.278 ± 0.106 μM , respectively. These two values are both in good agreement with the two reported experimental values: 0.025 μM [9] and 0.31 μM [51]. A possible interpretation of this agreement could be that subtle differences in the two experimental protocols yielded to the measurement of the two different acidic forms of cilomilast. This is somewhat confirmed in the case of npv. The two predicted IC_{50} values are 0.022 ± 0.011 and 1.256 ± 0.392 μM for the basic and the acidic forms of the carboxylic acid group, respectively. The predicted IC_{50} value of the carboxylic acid form again resembles more the experimental value (0.650) of Ref. [52] while the basic form resembles more the experimental value from Ref. [51]. It would be of course hazardous to generalize such findings, but, in our case, two

main points can be drawn: (1) the change of protonation of ionizable residues can greatly affect the computed binding energies and great care should be taken to assess such effects; (2) when multiple experimental values are available, it does not necessarily mean that some of them are "correct" or "wrong", but they can represent different states or be the results of applying different measurement protocols.

Conclusions

In this study, the MM-GB/SA method was used to estimate the free energy of binding, $\Delta G_{\text{binding}}$, of 15 PDE4B inhibitors. Since there exists a linear dependency between binding affinity (K_i) and IC_{50} , assuming that Michaelis-Menten constant (K_m), substrate concentrations [S], and experimental conditions are identical, the goal was to obtain a linear correspondence between $\log(IC_{50})$ values and $\Delta G_{\text{binding}}$.

The first step of this study was the database preparation with a combination of training and test ligand sets categorized based on their IC_{50} values. As a second step, a molecular docking study was performed. This yielded poor correlations between the docking scores, expressed as ΔG values, and the experimental IC_{50} ones. The results indicated that docking scores are not reliable enough to provide a linear dependency between IC_{50} values and $\Delta G_{\text{binding}}$.

After the docking process, 40 independent 1 ns long MD simulations were performed for the all representative poses of each AutoDock cluster. Our results show that, instead of a single long simulation, running multiple independent runs starting from the same structure but with different initial velocities can yield to statistically converged MM-GB/SA free energies of binding.

The binding free energy calculations were repeated for different solvation models: GB^{OBC} , GB^{OBC-2} , GB^{HCT} , GB^{GBneck} , and $GB^{GBneck2}$. The best results were obtained with the GB^{OBC} model, but other GB/SA models, except $GB^{GBneck2}$, lead to similar results. After checking the results according to best docked poses for each inhibitor, the linear trend was improved when all different clusters for each ligand were considered. A linear relationship between estimated IC_{50} versus experimental ones with $R^2 = 0.944$ was achieved. The reliability of our approach was verified with the test set that is here correctly predicted.

Overall, our study indicates that, to obtain a linear dependency between $\log(IC_{50})$ and MM-GB/SA results, it is important to take into account all different poses obtained after a docking process and not the best ones only. Such approach will be used in future studies to serve as benchmark for putative PDE4B ligands when no experimental value is available.

Acknowledgements G. Çifci, V. Aviyente received fundings from TUBITAK through Project 113Z001. G. Monard received fundings from CNRS through Project EDC25780. Computing resources used in this work were partially provided by the Centre de Calcul ROMEO of the Université de Reims Champagne-Ardenne, the State Planning Organization (DPT-2009K120520) and the Bogazici University Research Foundation (BAP-1856).

References

1. Torphy TJ (1998) Phosphodiesterase isozymes—molecular targets for novel antiasthma agents. *Am J Respir Crit Care Med* 157(2):351–370
2. Conti M, Jin SLC (2000) The molecular biology of cyclic nucleotide phosphodiesterases. *Prog Nucleic Acid Res Mol Biol* 63:1–38
3. Soderling SH, Beavo JA (2000) Regulation Of cAMP and cGMP signaling: new phosphodiesterases and new functions. *Curr Opin Cell Biol* 12(2):174–179
4. Callahan SM, Cornell NW, Dunlap PV (1995) Purification and properties of periplasmic 3'/5'-cyclic nucleotide phosphodiesterase—a novel zinc-containing enzyme from the marine symbiotic bacterium *Vibrio-Fischeria*. *J Biol Chem* 270(29):627–17, 632
5. Houslay MD, Milligan G (1997) Tailoring cAMP-signalling responses through isoform multiplicity. *Trends Biochem Sci* 22(6):217–224
6. Houslay MD, Sullivan M, Bolger GB (1998) The multienzyme PDE4 cyclic adenosine monophosphate-specific phosphodiesterase family: intracellular targeting, regulation, and selective inhibition by compounds exerting anti-inflammatory and antidepressant actions. *Adv Pharmacol* 44:225–342
7. Antoni FA (2000) Molecular diversity of cyclic AMP signalling. *Front Neuroendocrinol* 21(2):103–132
8. Xu RX, Hassell AM, Vanderwall D, Lambert MH, Holmes WD, Luther MA, Rocque WJ, Milburn MV, Zhao YD, Ke HM, Nolte RT (2000) Atomic structure of PDE4: insights into phosphodiesterase mechanism and specificity. *Science* 288(5472):1822–1825
9. Card GL, England BP, Suzuki Y, Fong D, Powell B, Lee B, Luu C, Tabrizizad M, Gillette S, Ibrahim PN, Artis DR, Bollag G, Milburn MV, Kim SH, Schlessinger J, Zhang KYJ (2004) Structural basis for the activity of drugs that inhibit phosphodiesterases. *Structure* 12(12):2233–2247
10. Houslay MD, Schafer P, Zhang KYJ (2005) Phosphodiesterase-4 as a therapeutic target. *Drug Discov Today* 10(22):1503–1519
11. Ke H, Wang H (2007) Crystal structures of phosphodiesterases and implications on substrate specificity and inhibitor selectivity. *Curr Top Med Chem* 7(4):391–403
12. Thompson WJ (1991) Cyclic-nucleotide phosphodiesterases - pharmacology, biochemistry and function. *Pharmacol Ther* 51(1):13–33
13. Mehats C, Andersen CB, Filopanti M, Jin SLC, Conti M (2002) Cyclic nucleotide phosphodiesterases and their role in endocrine cell signaling. *Trends Endocrinol Metab* 13(1):29–35
14. Giembycz MA (2000) Phosphodiesterase 4 inhibitors and the treatment of asthma—where are we now and where do we go from here? *Drugs* 59(2):193–212
15. Souness JE, Aldous D, Sargent C (2000) Immunosuppressive and anti-inflammatory effects of cyclic amp phosphodiesterase (PDE) type 4 inhibitors. *Immunopharmacology* 47(2–3):127–162
16. Huang Z, Ducharme Y, Macdonald D, Robichaud A (2001) The next generation of PDE4 inhibitors. *Curr Opin Chem Biol* 5(4):432–438

17. Sturton G, Fitzgerald M (2002) Phosphodiesterase 4 inhibitors for the treatment of COPD. *Chest* 121(5):192s–196s
18. Huai Q, Wang HC, Sun YJ, Kim HY, Liu YD, Ke HM (2003) Three-dimensional structures of PDE4D in complex with roliprams on inhibitor selectivity. *Structure* 11(7):865–873
19. Kang NS, Hong SJ, Chae CH, Yoo SE (2007) Comparative molecular field analysis (CoMFA) for phosphodiesterase (PDE) IV inhibitors. *J Mol Struct (THEOCHEM)* 820(1–3):58–64
20. Kongsted J, Ryde U (2009) An improved method to predict the entropy term with the MM/PBSA approach. *J Comput Aided Mol Des* 23(2):63–71
21. Rastelli G, Degliesposti G, Del Rio A, Sgobba M (2009) Binding estimation after refinement, a new automated procedure for the refinement and rescoring of docked ligands in virtual screening. *Chem Biol Drug Des* 73(3):283–286
22. Genheden S, Luchko T, Gusarov S, Kovalenko A, Ryde U (2010) An MM/3D-RISM approach for ligand binding affinities. *J Phys Chem B* 114(25):8505–8516
23. Rastelli G, Del Rio A, Degliesposti G, Sgobba M (2010) Fast and accurate predictions of binding free energies using MM-PBSA and MM-GBSA. *J Comput Chem* 31(4):797–810
24. Yuriev E, Agostino M, Ramsland PA (2011) Challenges and advances in computational docking: 2009 in review. *J Mol Recognit* 24(2):149–164. doi:10.1002/jmr.1077
25. Yuriev E, Ramsland PA (2013) Latest developments in molecular docking: 2010–2011 in review. *J Mol Recognit* 26(5):215–239. doi:10.1002/jmr.2266
26. Alexander RP, Warrelow GJ, Eaton MA, Boyd EC, Head JC, Porter JR, Brown JA, Reuberson JT, Hutchinson B, Turner P, Boyce B, Barnes D, Mason B, Cannell A, Taylor RJ, Zomaya A, Millican A, Leonard J, Morphy R, Wales M, Perry M, Allen RA, Gozzard N, Hughes B, Higgs G (2002) CDP840. A prototype of a novel class of orally active anti-inflammatory phosphodiesterase 4 inhibitors. *Bioorg Med Chem Lett* 12(11):1451–1456
27. Kuang R, Shue HJ, Blythin DJ, Shih NY, Gu D, Chen X, Schwerdt J, Lin L, Ting PC, Zhu X, Aslanian R, Piwinski JJ, Xiao L, Prelusky D, Wu P, Zhang J, Zhang X, Celly CS, Minnicozzi M, Billah M, Wang P (2007) Discovery of a highly potent series of oxazole-based phosphodiesterase 4 inhibitors. *Bioorg Med Chem Lett* 17(18):5150–5154
28. Zheng S, Kaur G, Wang H, Li M, Macnaughtan M, Yang X, Reid S, Prestegard J, Wang B, Ke H (2008) Design, synthesis, and structure-activity relationship, molecular modeling, and NMR studies of a series of phenyl alkyl ketones as highly potent and selective phosphodiesterase-4 inhibitors. *J Med Chem* 51(24):7673–7688
29. Guay D, Boulet L, Friesen RW, Girard M, Hamel P, Huang Z, Laliberte F, Laliberte S, Mancini JA, Muise E, Pon D, Styhler A (2008) Optimization and structure-activity relationship of a series of 1-phenyl-1,8-naphthyridin-4-one-3-carboxamides: identification of MK-0873, A potent and effective PDE4 inhibitor. *Bioorg Med Chem Lett* 18(20):5554–5558
30. Xu RX, Rocque WJ, Lambert MH, Vanderwall DE, Luther MA, Nolte RT (2004) Crystal structures of the catalytic domain of phosphodiesterase 4B complexed with AMP, 8-Br-AMP, and rolipram. *J Mol Biol* 337(2):355–365
31. Salter EA, Wierzbicki A (2007) The mechanism of cyclic nucleotide hydrolysis in the phosphodiesterase catalytic site. *J Phys Chem B* 111(17):4547–4552
32. Chen X, Zhao XY, Xiong Y, Liu JJ, Zhan CG (2011) Fundamental reaction pathway and free energy profile for hydrolysis of intracellular second messenger adenosine 3',5'-cyclic monophosphate (cAMP) catalyzed by phosphodiesterase-4. *J Phys Chem B* 115(42):208–212, 219
33. Dym O, Xenarios I, Ke H, Colicelli J (2002) Molecular docking of competitive phosphodiesterase inhibitors. *Mol Pharm* 61(1):20–25
34. Oliveira FG, Sant'Anna CMR, Caffarena ER, Dardenne LE, Barreiro EJ (2006) Molecular docking study and development of an empirical binding free energy model for phosphodiesterase 4 inhibitors. *Bioorg Med Chem* 14(17):6001–6011
35. Chen Z, Tian G, Wang Z, Jiang H, Shen J, Zhu W (2010) Multiple pharmacophore models combined with molecular docking: a reliable way for efficiently identifying novel PDE4 inhibitors with high structural diversity. *J Chem Inf Model* 50(4):615–625
36. Niu M, Dong F, Tang S, Fida G, Qin J, Liu K, Gao W, Gu Y (2013) Pharmacophore Modeling and virtual screening for the discovery of new type 4 cAMP phosphodiesterase (PDE4) inhibitors. *PLoS ONE* 8(12):e82, 360
37. Zhao P, Chen SK, Cai YH, Lu X, Li Z, Cheng YK, Zhang C, Hu X, He X, Luo HB (2013) The molecular basis for the inhibition of phosphodiesterase-4D by three natural resveratrol analogs. Isolation, molecular docking, molecular dynamics simulations, binding free energy, and bioassay. *Biochim et Biophys Acta* 1834(10):2089–2096. doi:10.1016/j.bbapap.2013.07.004
38. Voet D, Voet JG (1990) *Biochemistry*. Wiley, New York
39. Yung-Chi C, Prusoff WH (1973) Relationship between the inhibition constant (KI) and the concentration of inhibitor which causes 50 per cent inhibition (I50) of an enzymatic reaction. *Biochem Pharmacol* 22(23):3099–3108. doi:10.1016/0006-2952(73)90196-2
40. Zwanzig RW (1954) High-temperature equation of state by a perturbation method. I. Nonpolar gases. *J Chem Phys* 22(8):1420–1426
41. Lybrand TP, McCammon JA, Wipff G (1986) Theoretical calculation of relative binding-affinity in host guest systems. *Proc Natl Acad Sci USA* 83(4):833–835
42. Aqvist J, Medina C, Samuelsson JE (1994) New method for predicting binding-affinity in computer-aided drug design. *Protein Eng* 7(3):385–391
43. Kollman PA, Massova I, Reyes C, Kuhn B, Huo SH, Chong L, Lee M, Lee T, Duan Y, Wang W, Donini O, Cieplak P, Srinivasan J, Case DA, Cheatham TE (2000) Calculating structures and free energies of complex molecules: combining molecular mechanics and continuum models. *Acc Chem Res* 33(12):889–897
44. Wang JM, Morin P, Wang W, Kollman PA (2001) Use of MM-PBSA in reproducing the binding free energies to HIV-1 RT of TIBO derivatives and predicting the binding mode to HIV-1 RT of Efavirenz by docking and MM-PBSA. *J Am Chem Soc* 123(22):5221–5230
45. Beveridge DL, Dicapua FM (1989) Free-energy via molecular simulation - applications to chemical and biomolecular systems. *Annu Rev Biophys Biophys Chem* 18:431–492
46. Chipot C, Rozanska X, Dixit SB (2005) Can free energy calculations be fast and accurate at the same time?: binding of low-affinity, non-peptide inhibitors to the SH2 domain of the SRC protein. *J Comput Aided Mol Des* 19(11):765–770
47. Genheden S, Ryde U (2010) How to obtain statistically converged MM/GBSA results. *J Comput Chem* 31(4):837–846
48. Dal Piaz V, Giovannoni MP, Castellana C, Palacios JM, Beleta J, Domenech T, Segarra V (1998) Heterocyclic-fused 3(2H)-pyridazinones as potent and selective PDE IV inhibitors: further structure-activity relationships and molecular modelling studies. *Eur J Med Chem* 33(10):789–797
49. Liu T, Lin Y, Wen X, Jorissen RN, Gilson MK (2007) BindingDB: a web-accessible database of experimentally determined protein-ligand binding affinities. *Nucleic Acids Res* 35:D198–D201
50. Schrödinger, LLC (2015) The PyMOL molecular graphics system, version 1.8

51. Hersperger R, Bray-French K, Mazzoni L, Muller T (2000) Palladium-catalyzed cross-coupling reactions for the synthesis of 6,8-disubstituted 1,7-naphthyridines: a novel class of potent and selective phosphodiesterase type 4D inhibitors. *J Med Chem* 43(4):675–682
52. Wang H, Peng MS, Chen Y, Geng J, Robinson H, Houslay MD, Cai J, Ke H (2007) Structures of the four subfamilies of phosphodiesterase-4 provide insight into the selectivity of their inhibitors. *Biochem J* 408:193–201
53. The UniProt Consortium (2014) Activities at the universal protein resource (UniProt). *Nucleic Acids Res* 42(Database issue):D191–D198. doi:[10.1093/nar/gkt1140](https://doi.org/10.1093/nar/gkt1140)
54. Morris GM, Huey R, Lindstrom W, Sanner MF, Belew RK, Goodsell DS, Olson AJ (2009) AutoDock4 and AutoDockTools4: automated docking with selective receptor flexibility. *J Comput Chem* 30(16):2785–2791
55. Duan Y, Wu C, Chowdhury S, Lee MC, Xiong GM, Zhang W, Yang R, Cieplak P, Luo R, Lee T, Caldwell J, Wang JM, Kollman P (2003) A point-charge force field for molecular mechanics simulations of proteins based on condensed-phase quantum mechanical calculations. *J Comput Chem* 24(16):1999–2012
56. Case D, Darden T, Cheatham TE I, Simmerling C, Wang J, Duke R, Luo R, Walker R, Zhang W, Merz K, Roberts B, Hayik S, Roitberg A, Seabra G, Swails J, Goetz A, Kolossvy I, Wong K, Paesani F, Vanicek J, Wolf R, Liu J, Wu X, Brozell SR, Steinbrecher T, Gohlke H, Cai Q, Ye X, Wang J, Hsieh MJ, Cui G, Roe D, Mathews D, Seetin M, Salomon-Ferrer R, Sagui C, Babin V, Luchko T, Gusarov S, Kovalenko A, Kollman P (2012) AMBER 12. University of California, San Francisco
57. Sondergaard CR, Olsson MHM, Rostkowski M, Jensen JH (2011) Improved treatment of ligands and coupling effects in empirical calculation and rationalization of pK(a) values. *J Chem Theory Comput* 7(7):2284–2295
58. Jorgensen WL, Chandrasekhar J, Madura JD, Impey RW, Klein ML (1983) Comparison of simple potential functions for simulating liquid water. *J Chem Phys* 79(2):926–935
59. Goetz AW, Williamson MJ, Xu D, Poole D, Le Grand S, Walker RC (2012) Routine microsecond molecular dynamics simulations with AMBER on GPUs. 1. Generalized born. *J Chem Theory Comput* 8(5):1542–1555
60. Salomon-Ferrer R, Goetz AW, Poole D, Le Grand S, Walker RC (2013) Routine microsecond molecular dynamics simulations with AMBER on GPUs. 2. Explicit solvent particle Mesh Ewald. *J Chem Theory Comput* 9(9):3878–3888
61. Wang JM, Wolf RM, Caldwell JW, Kollman PA, Case DA (2005) Development and testing of a general AMBER force field. *J Comput Chem* 26(1):114
62. Ryckaert JP, Ciccotti G, Berendsen HJC (1977) Numerical—integration of cartesian equations of motion of a system with constraints—molecular-dynamics of N-alkanes. *J Comput Phys* 23(3):327–341
63. Ugur I, Marion A, Aviyente V, Monard G (2015) Why does Asn71 deamidate faster than Asn15 in the enzyme triosephosphate isomerase?: answers from microsecond molecular dynamics simulation and QM/MM free energy calculations. *Biochemistry* 54:1429–1439. doi:[10.1021/bi5008047](https://doi.org/10.1021/bi5008047)
64. Miller BR III, McGee TD Jr, Swails JM, Homeyer N, Gohlke H, Roitberg AE (2012) MMPBSA.py: an efficient program for end-state free energy calculations. *J Chem Theory Comput* 8(9):3314–3321. doi:[10.1021/ct300418h](https://doi.org/10.1021/ct300418h)
65. Hawkins G, Cramer C, Truhlar D (1995) Pairwise solute descreening of solute charges from a dielectric medium. *Chem Phys Lett* 246:122–129
66. Hawkins G, Cramer C, Truhlar D (1996) Parametrized models of aqueous free energies of solvation based on pairwise descreening of solute atomic charges from a dielectric medium. *J Phys Chem* 100:19,824–19,839
67. Tsui V, Case D (2001) Theory and applications of the generalized Born solvation model in macromolecular simulations. *Biopolymers (Nucl Acid Sci)* 56:275–291
68. Onufriev A, Bashford D, Case D (2004) Exploring protein native states and large-scale conformational changes with a modified generalized Born model. *Proteins* 55:383–394
69. Mongan J, Simmerling C, McCammon JA, Case DA, Onufriev A (2007) Generalized Born with a simple, robust molecular volume correction. *J Chem Theory Comput* 3:156–169
70. Nguyen H, Roe DR, Simmerling C (2013) Improved generalized born solvent model parameters for protein simulations. *J Chem Theory Comput* 9(4):2020–2034
71. Weiser J, Shenkin P, Still W (1999) Approximate atomic surfaces from linear combinations of pairwise overlaps (LCPO). *J Comput Chem* 20:217–230
72. Genheden S, Kuhn O, Mikulskis P, Hoffmann D, Ryde U (2012) The normal-mode entropy in the MM/GBSA method: Effect of system truncation, buffer region, and dielectric constant. *J Chem Inf Model* 52(8):2079–2088. doi:[10.1021/ci3001919](https://doi.org/10.1021/ci3001919)
73. Hou T, Wang J, Li Y, Wang W (2011) Assessing the performance of the MM/PBSA and MM/GBSA methods. 1. The accuracy of binding free energy calculations based on molecular dynamics simulations. *J Chem Inf Model* 51(1):69–82. doi:[10.1021/ci100275a](https://doi.org/10.1021/ci100275a)
74. Genheden S (2011) MM/GBSA and LIE estimates of host-guest affinities: dependence on charges and solvation model. *J Comput Aided Mol Des* 25(11):1085–1093. doi:[10.1007/s10822-011-9486-1](https://doi.org/10.1007/s10822-011-9486-1)
75. Genheden S, Ryde U (2011) Comparison of the efficiency of the LIE and MM/GBSA methods to calculate ligand-binding energies. *J Chem Theory Comput* 7(11):3768–3778. doi:[10.1021/ct200163c](https://doi.org/10.1021/ct200163c)
76. Hayes JM, Archontis G (2012) Molecular dynamics—Studies of synthetic and biological macromolecules, InTech, chap MM-GB(PB)SA calculations of protein-ligand binding free energies
77. Genheden S, Ryde U (2015) The MM/PBSA and MM/GBSA methods to estimate ligand-binding affinities. *Expert Opin Drug Discov* 10(5):449–461. doi:[10.1517/17460441.2015.1032936](https://doi.org/10.1517/17460441.2015.1032936)
78. Nguyen H, Maier J, Huang H, Perrone V, Simmerling C (2014) Folding simulations for proteins with diverse topologies are accessible in days with a physics-based force field and implicit solvent. *J Am Chem Soc* 136(40):959–962. doi:[10.1021/ja5032776](https://doi.org/10.1021/ja5032776)